Published in: Colloids and Surfaces A : Physicochemical and Engineering Aspects (2004), vol. 241, iss. 1-3, pp. 201-206.
Status: Postprint (Author's version).

Image analysis of X-ray microtomograms of Pd-Ag/SiO_2 xerogel catalysts supported on Al_2O_3 foams

S. Blacher[a], A. Léonard[a], B. Heinrichs[a], N. Tcherkassova[a], F. Ferauche[a], M. Crine[a], P. Marchot[a], E. Loukine[b], J.-P. Pirard[a]

[a] *Laboratory of Chemical Engineering, Department of Applied Chemistry, University of Liège, Sart-Tilman B6a, B-4000 Liège, Belgium*
[b] *Department of Chemical Technology of Silicates, Chemical Technology of Refractory Non-metallic and Silicate Materials, D. Mendeleev University of Chemical Technology of Russia, Miusskaya Square 9, 1254047 Moscow, Russia*

Abstract

In order to preshape and mechanically strengthen, Pd-Ag/SiO_2 xerogel catalysts were carried out in $A1_20_3$ foams (pore-sizes ~40 µm). The final material consists of a Pd-Ag/SiO_2 xerogel immobilized in the open cells of the alumina foam. The localization of the xerogel catalyst in alumina foams of various pore structure was studied by X-ray microtomography. The three-dimensional (3D) porous structure was reconstructed from the consecutive cross-sections obtained by this technique. Total porosity, porous density distribution, and pore-size distribution were determined by image analysis on the free and impregnated supports. Our results show that the success of the used impregnation technique depends on the pore structure of the support.

Keywords: Alumina foam; X-ray microtomography; Image analysis; Xerogel; Impregnation

1. INTRODUCTION

Previously, the synthesis by cogelation, the characterization and the catalytic properties of Pd-Ag/SiO2 xerogel catalysts have been reported [1,2]. This cogelled catalyst is devoted to the selective hydrodechlorination of chlorinated alkanes into alkenes. This reaction is particularly interesting from both an economical and environmental point of view in comparison with the present incineration of chlorinated industrial wastes [3,4]. The extrapolation of the catalyst synthesis to the industrial scale requires preshaping and a mechanical strengthening of this material. To achieve this goal, gelation of the initial solution containing Pd, Ag, and SiO2 precursors has been carried out in the highly porous structure of Al_2O_3 foams (pore-sizes ~40 µm). Those foams have been chosen for their high strength and porosity. After aging of the gel, drying under vacuum, and thermal treatments, a wide pore range xerogel (~ 1-l00nm), trapping Pd-Ag alloy nanocrystallites inside primary silica particles, is itself immobilized in the open cells of the alumina foam.

The knowledge of the localization of the xerogel catalyst on the alumina foam is important to understand the catalytic properties of the whole system. This implies determining the local porosity variations before and after the impregnation process. Mercury porosimetry is commonly used to measure pore volume and pore-size distribution of highly porous materials. However, the use of this technique is not appropriated in the present case. Indeed, on the one hand, mercury porosimetry is limited to maximum pore-sizes of 75 µm and, on the other hand, the foam porous structure is so open that mercury would not intrude the sample but would flow through the porous structure.

Recently, some of us used X-ray microtomography coupled with image analysis techniques to characterize the texture of soft highly porous materials [5,6]. X-ray microtomography is non-destructive, easy to implement and allows covering a wide range of characteristic scales from tens of microns up to the size of the sample (1-2 cm). This technique allows visualizing the porous structure. Indeed, the consecutive cross-sections obtained by this technique can be used to perform a three-dimensional (3D) image reconstruction. Image analysis on the reconstructed images can be used to quantify the porous structure.

In this work, the texture of the internal surface of alumina foams before and after Pd-Ag/SiO_2 xerogel impregnation is studied by X-ray microtomography coupled with image analysis. X-ray microtomography technique is briefly described as well as the algorithms used for 3D image analysis.

Published in: Colloids and Surfaces A : Physicochemical and Engineering Aspects (2004), vol. 241, iss. 1-3, pp. 201-206.
Status: Postprint (Author's version).

2. EXPERIMENTAL

2.1. Preparation of Pd-Ag/SiO_2 xerogels supported on α-Al_2O_3 foams

2.1.1. Initial sol-gel solution

The initial sol-gel solution into which α-alumina foams have been dipped is prepared as follows. To a suspension containing 0.121 g of insoluble palladium acetylacetonate powder ($Pd(acac)_2$, Aldrich 20, 901-5) and 0.131 g of insoluble silver acetate powder (AgOAc, Aldrich 20, 437-4) in 13.03 ml of ethanol denaturized with 0.5% of diethyl phthalate (DEP), 0.51 ml of [3-(2-aminoethyl)aminopropyl]trimethoxysilane (EDAS, ABCR 1760-24-3, industrial grade) is added. This mixture is stirred at ambient temperature in a closed vessel during 1 h to allow EDAS to form complexes with Pd and Ag [1]. Tetraethoxysilane, 9.44ml, (TEOS, ABCR 78-10-4, industrial grade) is then added. Finally, a solution containing 3.97 ml of aqueous 0.2M NH3 in 13.03 ml of denaturized ethanol is slowly added under vigorous stirring.

Fig. 1: *X-ray tomographic cross-sections of free (a), impregnated (b), and calcinated (c) alumina foam and their corresponding binary images (d)-(f).*

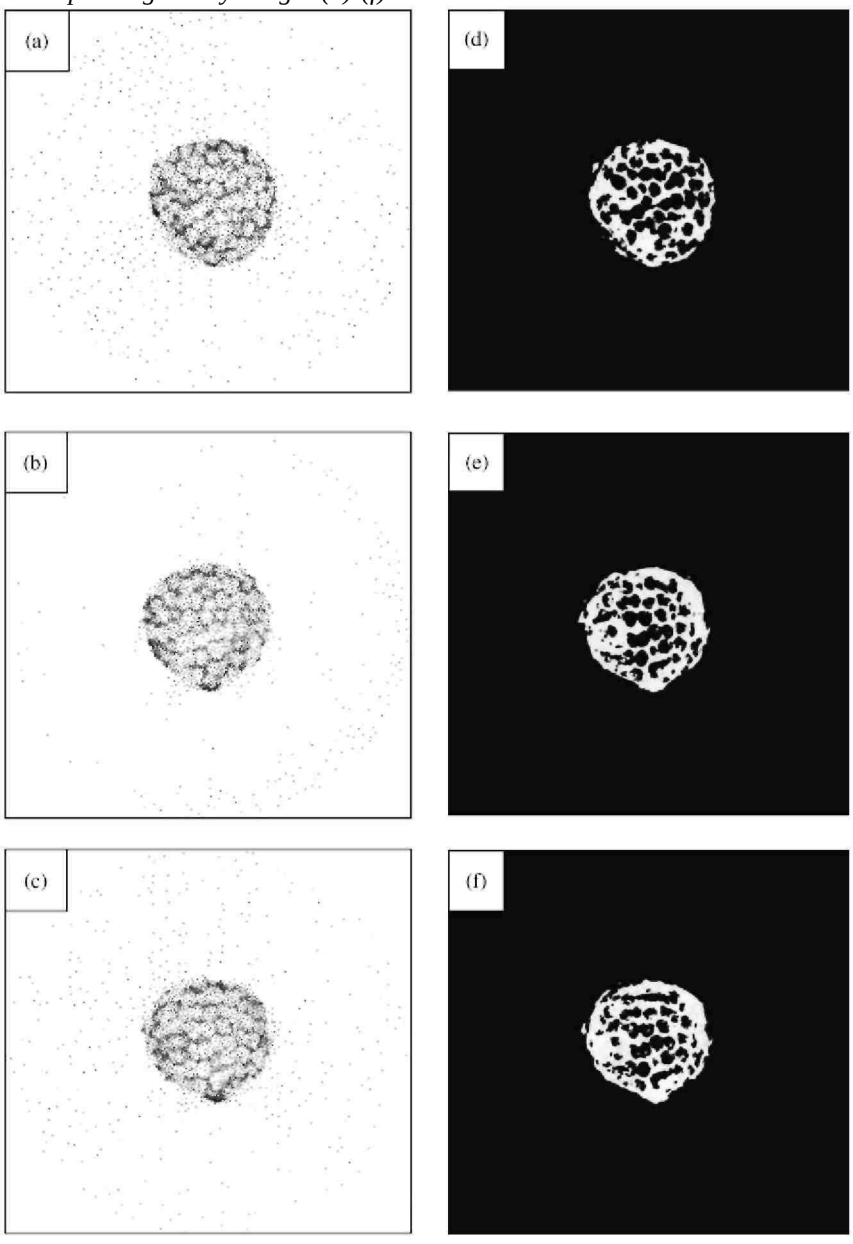

2.1.2. Impregnation of alumina foams

Three α-alumina foams which differ by their porosities (AL1, AL2, AL3) are plunged into the vessel containing the above described sol-gel solution immediately after the introduction of aqueous ammonia, i.e., when the solution is still liquid. The vessel is then closed tightly and heated to 70 °C for 3 days (gelation and aging).

2.1.3. Drying

After aging, the gel containing the α-Al_2O_3 foams is dried under vacuum according to the following procedures—the vessel is opened and put into a drying oven heated to 80 °C, and the pressure is slowly decreased (to prevent gel bursting) to 1200 Pa after 18 h. At 1200 Pa, the temperature is increased up to 150 °C and the gel is maintained under those conditions during 32 h. The impregnated α-alumina foams are then removed from the excess gel and submitted to X-ray tomography.

2.1.4. Calcination

Samples are heated to 400 °C at a rate of 120 °C h^{-1} under flowing air (1.8Nlh^{-1}); this temperature in air (9Nlh^{-1}) is then maintained for 12 h

Fig. 2: *3D image reconstruction of free AL1 (a), AL2 (b), and AL3 (c) and impregnated AL1 (d), AL2 (e), and AL3 (f) alumina foams.*

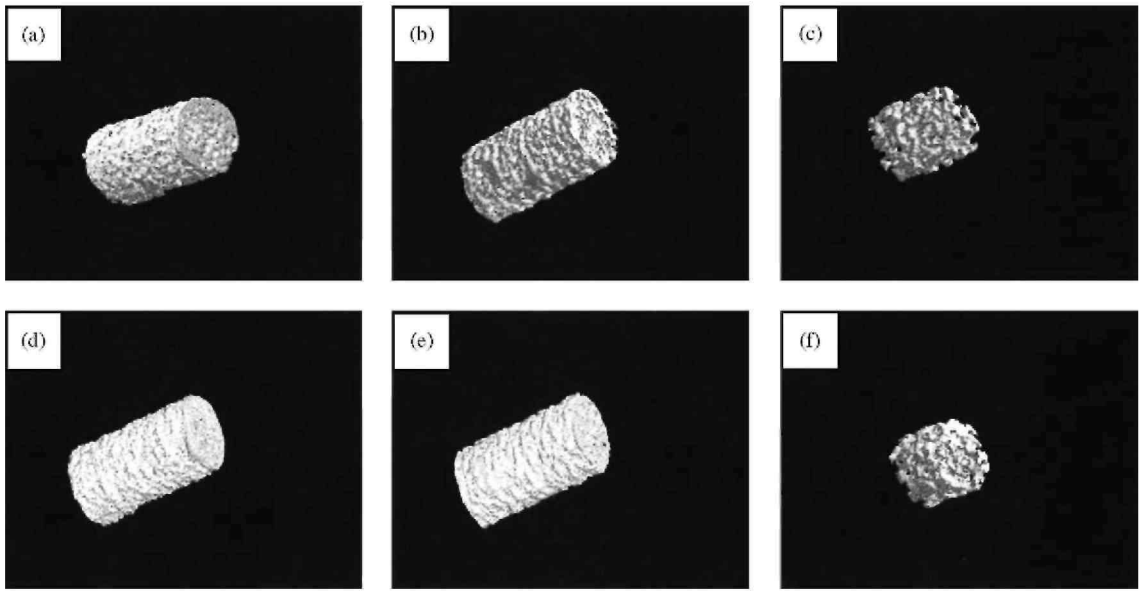

2.2. X-ray microtomograph

The X-ray tomographic device used in this study is a "Skyscan-1074 X-ray scanner" (Skyscan, Belgium). Advanced technical details about its conception and operation are described by Sasov and Van Dyck [7]. The X-ray source operates at 40 kV and 1 mA. The detector is a 2D, 768 pixels x 576 pixels, 8-bit X-ray camera with a spatial resolution of 41 µm. The rotation step is fixed at the minimum, 0.9°, in order to improve image quality. Once the sample is placed into the microtomograph, the scanning is performed, allowing the investigation of a height of approximately 2 cm. Cross sections separated by 205 µm are then reconstructed using a cone-beam reconstruction software. That means 83, 88, and 48 cross sections, respectively for the samples AL1, AL2, AL3.

2.3. Image analysis

The 3D images, obtained from cross-section X-ray microtomography images reconstruction, were processed and analyzed using basic tools of mathematical morphology and signal processing [8,9]. Specific programs were developed using Aphelion3.2f (Adcis S.A) and Matlab softwares, with image analysis toolbox version 6.0 from Matworks. The 3D images visualization was obtained by stacking a series of 2D binary cross section images separated by 0.41 mm using the 3D visualization software package provided by Skyscan.

Published in: Colloids and Surfaces A : Physicochemical and Engineering Aspects (2004), vol. 241, iss. 1-3, pp. 201-206.
Status: Postprint (Author's version).

2.4. Image processing and measurements

Grey level cross section images were first binarised using Otsu's method [10]. With this method, the threshold level is chosen automatically so as to maximize the interclass variance and to minimize the intraclass variance of the thresh-olded black (pores) and white (support) pixels. Then, 3D binary images were reconstructed from binary sections.

On 3D binary images, the following measurements were performed:

(a) The total porosity *(δ)*, defined as *8* = number of pixels characteristic of the pores (V_p)/(number of pixels characteristic of the pores + number of pixels characteristic of the support). To determine V_p, the 3D image is reversed so as the pores correspond to white measurable pixels. To determine the total volume of the sample, a closing and hole-fill transformations were applied on the original 3D binary image in order to complete the external surface and to fill the pores. Then, the total volume of the image is determined.

(b) The pore density distribution (δ_L) defined as $\delta_L(d)$ = number of pixels characteristic of the pores in a layer located at a distance *d* of the center of the sample/total number of pixels which form that layer. For this kind of measurement the shape of the layers must be chosen in function of the pore structure. As 3D image visualization of samples reveals a roughly isotropic structure, layers were defined by the volume in between successive cylinders defined as the boundaries of the sample eroded n = 1, 2, 3,... times, with an octahedron of 1 pixel diameter.

(c) The pore-size distribution. As the pores have a continuous and open structure, standard granulometry cannot be applied. Then, we calculate the opening size distribution G(λ) (8) which allows assigning a size to both continuous and individual particles. When an opening transformation is performed on a binary image, objects whose size is smaller than a convex structural object of known size, are removed. This transformation simulates the physical mechanism of sieving. After a series of opening transformations with convex structural elements of larger and larger sizes, the opening size distribution is obtained. Let *f(X)* be the indicator function of a random stationary set *X* represented here through the 3D image of the support. The opening size distribution G(λ) can be calculated using the following algorithm:

$$G(\lambda) = \frac{A(X) - A(O^{\lambda B}(X))}{A(X)} \qquad (1)$$

where *A(X)* is the area of *X*, i.e., the number of pixels which make up the studied phase and $O^{\lambda B}(X)$, the opening transformation of *X* by a structural element. The algorithm of Eq. (1) was applied to the reversed 3D image, i.e., to a 3D image in which pores correspond to white measurable pixels and the support to black pixels. As the pore seems roughly isotropic on the images, we have chosen, for simplicity, a sphere as a structural element (octahedron on the image). Thus $A(O^{\lambda B}(X))$ corresponds to the volume formed by the elements of the phase *X* in which a sphere of radius greater or equal than λ can be inscribed. The first derivative of the opening size distribution (G(λ)) gives the granulometry density which we have characterized by the position of their maximum (λ_m) and the full width at half maximum (FWHM). These parameters are usually used to describe empirical distributions.

Table 1: *Porosity and granulometry density for the free, impregnated catalyst and calcined catalyst supports*

Sample	Porosity(*δ*)			Granulometry density (g(λ))					
	δ	*δ**	*δ***	λ_m (mm)	FWHM (mm)	λ_m* (mm)	FWHM* (mm)	λ_m** (mm)	FWHM** (mm)
AL1	0.56	0.41	0.40	0.15	0.13	0.15	0.12	0.15	0.12
AL2	0.62	0.50	0.49	0.16	0.16	0.15	0.13	0.15	0.14
AL3	0.73	0.67	0.67	0.17	0.25	0.17	0.21	0.17	0.22

δ, *δ** and *δ*** are the porosity of the free support, the impregnated support and the calcined catalyst, respectively. λ_m, λ_m* and λ_m** are the positions of the maximum and FWHM*, FWHM* and FWHM** the full width at half maximum of g(λ) for the free support, the impregnated support and the calcined catalyst, respectively.

Published in: Colloids and Surfaces A : Physicochemical and Engineering Aspects (2004), vol. 241, iss. 1-3, pp. 201-206.
Status: Postprint (Author's version).

3. RESULTS AND DISCUSSION

The three α-Al_2O_3 foams (AL1, AL2, AL3) used in this study were characterized before and after impregnation with Pd-Ag/SiO_2 xerogel catalysts as well as after calcination. Fig. 1 shows, as an example, a tomographic cross section image of the original (Fig. 1a), impregnated (Fig. 1b) and calcined (Fig. 1c) AL1 foam and their corresponding binary images (Fig. 1d-f, respectively). A simple inspection of those images indicates that porosity seems to increase from the external border towards the center of the sample and that the impregnated and calcined cross section images are less porous than the original support.

The same trends is observed on the cross section images of the AL2 and AL3 foams (not shown). The 3D reconstructed images from 2D binary cross section images of the three free and impregnated foams (Fig. 2) seem to indicate that AL3 foams (Fig. 2c) have a more open structure than AL1 and AL2 foams (Fig. 2a and b, respectively).

The total porosity of the original (δ), impregnated (δ^*) and calcined (δ^{**}) foams were measured by the procedure described in Section 2.3 (a) (see Table 1). These measurements show that (a) the porosity of the free foams increases from AL1 to AL3, (b) the porosity decrease by 27% for AL1, 19% for AL2 and 8% for AL3, after impregnation and (c) the porosity is not modified by the calcination of the impregnated samples.

Fig. 3: *Pore-density distribution for free and impregnated alumina foams for AL1 (a), AL2 (b), and AL3 (c).*

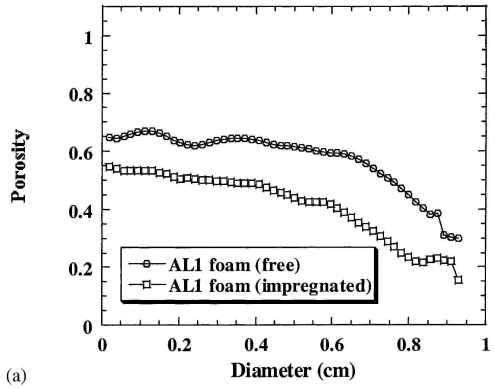

(a)

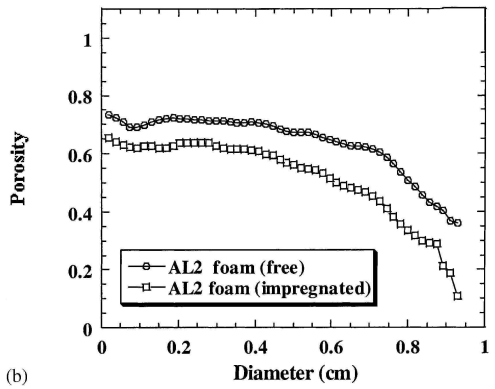

(b)

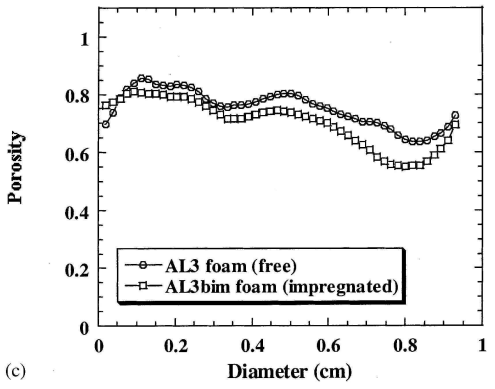

(c)

Published in: Colloids and Surfaces A : Physicochemical and Engineering Aspects (2004), vol. 241, iss. 1-3, pp. 201-206.
Status: Postprint (Author's version).

In order to characterize the pore distribution of the free foams and the changes induced by impregnation, the pore-density distribution was measured using the methodology described in Section 2.3 (b). The following trends were observed (Fig. 3a-c):

(a) for the three free supports (AL1, AL2, AL3), porosity decreases from the center to the external border. The same behavior is observed for impregnated and calcined (not shown) samples;

(b) the curves obtained for the free and the corresponding impregnated samples have almost the same shape;

(c) curves corresponding to the impregnated sample are shifted lower down, i.e., towards a lower porosity. The shift decreases slightly from the border to the center of the sample;

(d) the largest shift corresponds to AL1, the lowest shift corresponds to AL3.

Fig. 4: *Granulometry density of free alumina foams (a) and comparison between free and impregnated AL1 (b), AL2 (c), and AL3 (d) alumina foams.*

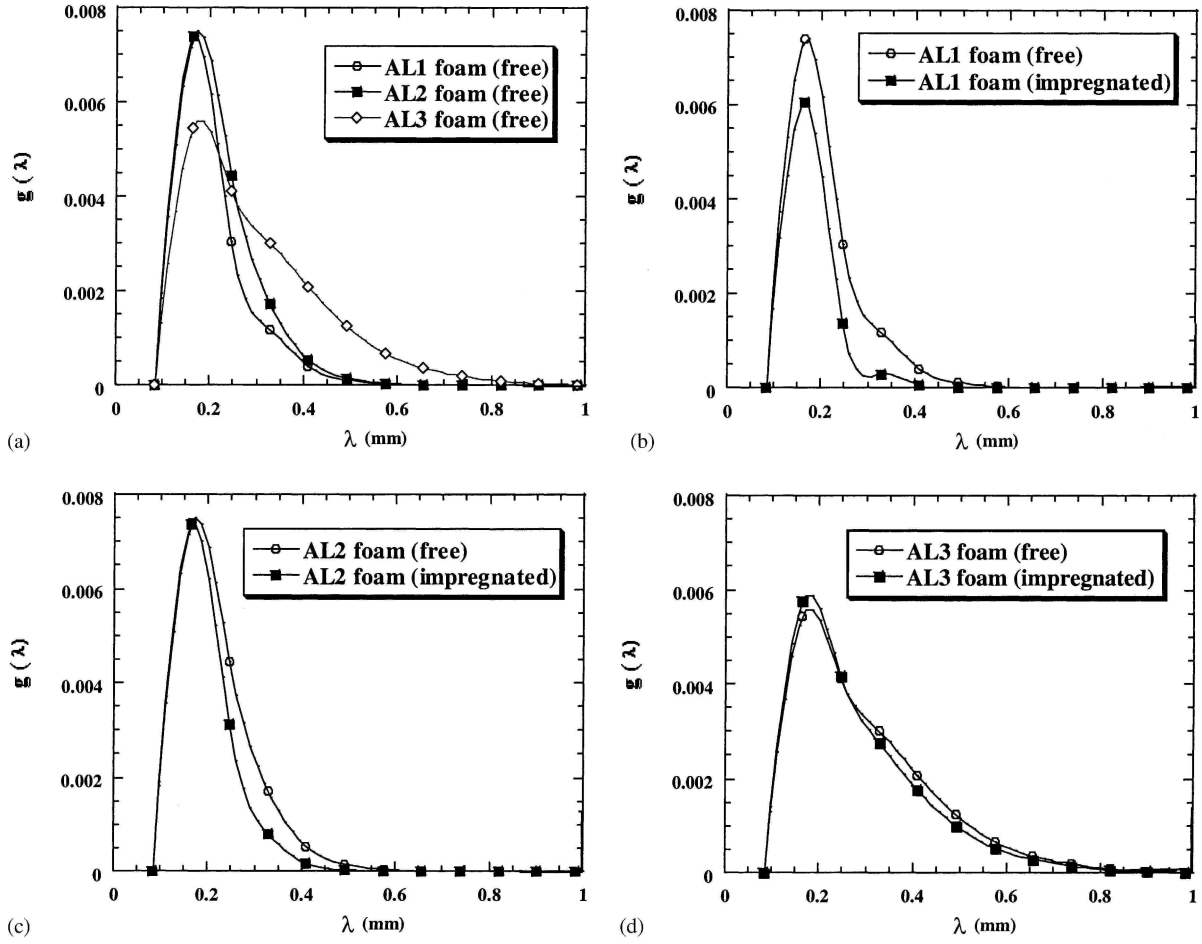

The fact that free and impregnated curves have almost the same shape implies that impregnation decreases the porosity homogeneously everywhere in the support. In other words, the xerogel catalyst fills the support homogeneously. A low shift of the pore-density distribution corresponds to a low catalyst load. For the AL3 sample, curves are shifted near the border only (Fig. 3c) which signifies that homogeneous impregnation process has failed.

The granulometry density g(λ), which is the first derivative of the opening size distribution G(λ), of the free supports and the impregnated ones are presented in Fig. 4a-d. To describe those functions, λ_m and the FWHM have been determined. AL1 and AL2 free foams (Fig. 4a) present similar narrow granulometry density distributions, with very close values of λ_m's and FWHMs (see Table 1). On the contrary, for the AL3 free foam, the granulometry density curve presents a tail towards the large sizes, which indicates that pore-sizes spread in a

larger range. A comparison between the granulometry density distributions of free and impregnated foams (Fig. 4b-d) indicates that, for AL1 and AL2 samples, λ_m is lower after impregnation (see Table 1). As expected, no change for the AL3 foam is observed before and after impregnation (see Fig. 4d and Table 1). It must be noticed that the opening size distribution and the derived granulometry density used in this study, induced a shift of the true size distribution towards lower values. Indeed, if for example, a pore is formed by two parts nearly convex, separated by a thin "isthmus," it will be transformed after an opening transformation into two pores of lower diameter. In this case, an artificial decrease of the average diameter distribution is produced. A high decrease corresponds to a high degree of pores irregularity. In fact, this kind of measurement is specially useful for comparative studies as it is presented in this work.

4. CONCLUSION

This study shows that X-ray microtomography coupled with image analysis is a valuable method to explore the texture variation of highly porous inorganic foams resulting from their impregnation with xerogel catalysts. The methodology used allows selecting the foam structures suitable for impregnation. This is a powerful tool to validate the strategy we developed to preshape and strengthen xerogel catalysts. Further catalytic tests will provide more insight into the relationship between the morphology of the structured Pd-Ag/SiO_2 xerogel/α-Al_2O_3 foam and its catalytic performances. The latter study will be very important to assess the industrial viability of cogelled xerogels when preshaped and strengthened by means of inorganic foams.

Acknowledgements

The authors thank the Ministry of "Région Wallonne" (DGTRE), Belgium and the Ministry of the "Communauté française de Belgique," Belgium (Action de Recherche Concertée 00/05-265) for their financial support.
A. Léonard is also grateful to the FNRS (National Fund for Scientific Research, Belgium) for a Scientific Research Worker position.

References

[1] B. Heinrichs, P. Delhez, J.-P. Schoebrechts, J.-P. Pirard, J. Catal. 172 (1997) 322.

[2] B. Heinrichs, S. Lambert, C. Alié, J.-P. Pirard, G. Beketov, V. Nehasil, N. Kruse, Stud. Surf. Sci. Catal. 143 (2002) 25.

[3] T.N. Kalnes, R.B. James, Environ. Prog. 7 (1988) 185.

[4] P. Delhez, B. Heinrichs, J.-P. Pirard, J.-P. Schoebrechts, US Patent no. 6,072,096 (2000).

[5] A. Léonard, S. Blacher, P. Marchot, M. Crine, Drying Tech. 20 (2002) 1053.

[6] S. Blacher, V. Maquet, A. Léonard, G. Chapelle, M. Crine, R. Jérôme, J.-P. Pirard, in: F. Rogriguez-Reinoso, B. McEnaney, J. Rouquerol, K. Unger (Eds.), Characterizations of Porous Solids, vol. VI, Elsevier, Amsterdam, 2002, p. 331.

[7] A. Sasov, D. Van Dyck, J. Microsc. 191 (1998) 151.

[8] J. Serra, Image Analysis and Mathematical Morphology, vol. 1, Academic Press, New York, 1982.

[9] M. Coster, J.L. Chermant, Précis d'analyse d'images, CNRS, Paris, 1985.

[10] N. Otsu, IEEE Trans. Syst. Man Cybern. 9 (1979) 62.